Manuscript prepared for Atmos. Chem. Phys. Discuss.
with version 2.2 of the LaTeX class copernicus_discussions.cls.
Date: 31 January 2011

Inverse modelling of European N_2O emissions: assimilating observations from different networks

M. Corazza[1], P. Bergamaschi[1], A. T. Vermeulen[2], T. Aalto[3], L. Haszpra[4], F. Meinhardt[5], S. O'Doherty[6], R. Thompson[7], J. Moncrieff[8], E. Popa[2], M. Steinbacher[9], A. Jordan[10], E. Dlugokencky[11], C. Brühl[12], M. Krol[13], and F. Dentener[1]

[1]European Commission Joint Research Centre, Institute for Environment and Sustainability, 21027 Ispra (Va), Italy
[2]Energy research Centre of the Netherlands (ECN), Petten, The Netherlands
[3]Finnish Meteorological Institute (FMI), Helsinki, Finland
[4]Hungarian Meteorological Service, Budapest, Hungary
[5]Umweltbundesamt (UBA), Messstelle Schauinsland, Kirchzarten, Germany
[6]School of Chemistry, University of Bristol, Bristol, UK
[7]Laboratoire des Sciences du Climat et de l'Environment (LSCE), Gif sur Yvette, France
[8]Edinburgh University, Edinburgh, UK

Correspondence to: M. Corazza (matteo.corazza@jrc.ec.europa.eu)

[9]Swiss Federal Laboratories for Materials Science and Technology (Empa),
Duebendorf, Switzerland
[10]Max Planck Institute for Biogeochemistry, Jena, Germany
[11]NOAA Earth System Research Laboratory, Global Monitoring Division, Boulder, CO, USA
[12]Max Planck Institute for Chemistry, Mainz, Germany
[13]Wageningen University and Research Centre (WUR), Wageningen, The Netherlands

Received: 31 August 2010 – Accepted: 11 October 2010 – Published: [redacted]

Correspondence to: M. Corazza (matteo.corazza@jrc.ec.europa.eu)

Published by Copernicus Publications on behalf of the European Geosciences Union.

Abstract

We describe the setup and first results of an inverse modelling system for atmospheric N_2O, based on a four-dimensional variational (4DVAR) technique and the atmospheric transport zoom model TM5. We focus in this study on the European domain, utilizing a comprehensive set of quasi-continuous measurements over Europe, complemented by N_2O measurements from the Earth System Research Laboratory of the National Oceanic and Atmospheric Administration (NOAA/ESRL) cooperative global air sampling network. Despite ongoing measurement comparisons among networks parallel measurements at a limited number of stations show that significant offsets exist among the different laboratories. Since the spatial gradients of N_2O mixing ratios are of the same order of magnitude as these biases, the direct use of these biased datasets would lead to significant errors in the derived emissions. Therefore, in order to also use measurements with unknown offsets, a new bias correction scheme has been implemented within the TM5-4DVAR inverse modelling system, thus allowing the simultaneous assimilation of observations from different networks. The N_2O bias corrections determined in the TM5-4DVAR system agree within ~0.1 ppb (dry-air mole fraction) with the bias derived from the measurements at monitoring stations where parallel NOAA discrete air samples are available. The N_2O emissions derived for the northwest European and east European countries for 2006 show good agreement with the bottom-up emission inventories reported to the United Nations Framework Convention on Climate Change (UNFCCC). Moreover, the inverse model can significantly narrow the uncertainty range reported in N_2O emission inventories for these countries, while the lack of measurements does not allow ~~for better~~to reduce the uncertainties of emission estimates in southern Europe.

Several sensitivity experiments were performed to test the robustness of the results. It is shown that also inversions without detailed a priori spatio-temporal emission distributions are capable to reproduce major regional emission patterns within the footprint of the existing atmospheric network, demonstrating the strong constraints of the atmospheric observations on the derived emissions.

1 Introduction

Atmospheric mixing ratios of nitrous oxide (N_2O) have significantly increased since preindustrial times and continue to increase by 0.2 to 0.3%/yr (IPCC, 2007). N_2O is the fourth most important anthropogenic greenhouse gas (GHG) after CO_2, CH_4 and CFC-12, with a global warming potential of almost 300 relative to CO_2 over a 100 yr time horizon (IPCC, 2007). Furthermore, N_2O is considered to become the most important ozone depleting gas of the 21st century, after the drastic abatement of the chlorofluorocarbons in recent years (Ravishankara et al., 2009). A significant part of N_2O removal in the stratosphere ($\sim$10%) is caused by reaction with electronically excited oxygen atoms, and about half of those reactions produce nitric oxide, which is part of a catalytic cycle that destroys ozone (Crutzen, 1974; Nevison and Holland, 1997).

The current increase of atmospheric N_2O mixing ratios of 0.73 ± 0.06 ppb/yr is equivalent to an imbalance between sources and sinks of about 3.5 TgN/yr (Hirsch et al., 2006; Hall et al., 2002). With an atmospheric lifetime of 122 ± 24 years, as derived by Volk et al. (1997) using stratospheric measurements, the global total sinks of N_2O are estimated to be 12.5 ± 2.5 TgN/yr, and the sources from surface emissions $\sim$16 TgN/yr (Hirsch et al., 2006). Based on preindustrial N_2O mixing ratios of 265–280 ppb, Hirsch et al. (2006) estimate the preindustrial N_2O sources to be about 11 TgN/yr.

Atmospheric measurements combined with inverse atmospheric models can provide independent "top-down" emission estimates of atmospheric trace gases. Inverse modelling has been widely applied to CO_2 and CH_4 (IPCC, 2007), while only relatively few studies are available for N_2O. Major challenges for inverse modelling of N_2O include (1) the very small gradients of N_2O (and hence low signal-to-noise ratio of the measurements constraining the inversion), (2) potential biases between measurements from different laboratories, (3) the difficulty to simulate the stratospheric sink and stratosphere-troposphere exchange realistically, and (4) large spatial and temporal variability of N_2O emissions. The first inverse analysis of the global N_2O cycle was presented by Prinn et al. (1990) based on a 9-box model and atmospheric observations from the ALE-GAGE (Atmospheric Lifetime Experiment – Global Atmospheric Gases

Experiment) network for 1978–1988. They concluded that beside the use of fertilizer and fossil fuel combustion in mid latitudes, tropical sources (probably from tropical land use change) are likely to play an important role for the global budget and the observed N_2O increase. The more recent studies of Hirsch et al. (2006) and Huang et al. (2008), based on 3-D global inverse models, suggest an even larger contribution of the tropical sources between 0 and 30° N to the global total (50–64% using observations from the NOAA – National Oceanic and Atmospheric Administration – network for 1998–2001 – Hirsch et al., 2006; 40–56% using the observations from the AGAGE – Advanced GAGE – network for 1997–2005 – Huang et al., 2008) than estimated by Prinn et al. (1990 – 32–39% for 1978–1988) – or estimated by measurement based (bottom-up) inventories (34%; Bouwman et al., 1995).

In addition, to improve our knowledge about global GHG cycles, inverse modelling is an important tool for regional emission estimates and independent verification of international agreements on emission reductions, such as the United Nations Framework Convention on Climate Change (UNFCCC) and the Kyoto Protocol (Bergamaschi, 2007; IPCC, 2000). First inverse modelling (top-down) estimates of European N_2O emissions were provided by Ryall et al. (2001) and Manning et al. (2003), using N_2O observations from Mace Head and the NAME Lagrangian particle model. Their estimates for northwest European countries agreed within ∼30% or better with emissions reported to UNFCCC. A model-independent "top-down" approach using the ^{222}Rn tracer method presented by Messager et al. (2008), also agreed well with bottom-up emission estimates. It needs to be emphasized, however, that top-down approaches generally estimate total emissions, while emissions reported to UNFCCC cover only anthropogenic emissions. Hence, for quantitative comparisons, good bottom-up estimates of the natural sources are needed.

While the above European top-down emission estimates are based on one single station (Mace Head), improved emission estimates require the use of further atmospheric measurements, to provide better coverage of the European domain. Additional continuous N_2O measurements are now available from ~~various~~10 European monitoring stations, including ~~a number of~~5 tall towers, which where setup in the framework of the European RTD (Research and Technology Development) project CHIOTTO (Continuous HIgh-precisiOn Tall Tower Observations

of greenhouse gases). Despite ongoing measurement comparisons among the different laboratories, significant offsets still exist among the different networks, which are directly apparent from the comparison with flask samples from the NOAA/ESRL (Earth System Research Laboratory) network, which are available for some European monitoring stations.

Here we describe the setup of a four-dimensional variational (4DVAR) inverse modelling system for N_2O based on the atmospheric transport zoom model TM5. The TM5-4DVAR system was originally developed and applied to CH_4 (Meirink et al., 2008; Bergamaschi et al., 2009, 2010). The most important update for N_2O is the implementation of a bias correction scheme to correct for the N_2O measurement offsets, which is a central prerequisite for the simultaneous assimilation of observations from different networks.

In this paper, we present first N_2O inversions for 2006 focussing on the European scale using continuous measurements from the various new European monitoring stations. The major objective of this paper is to demonstrate that our system can derive realistic bias corrections, assuming that the measurement offsets are constant over the inversion time period, and that after bias correction, inversions provide significant information on emissions. Furthermore, we investigate the impact of the applied a priori emission inventories on the results and compare them with a sensitivity inversion without using detailed a priori knowledge on the emissions, similar to experiments carried out for CH_4 (Bergamaschi et al., 2009, 2010). Such "free inversions", which are largely driven by the atmospheric measurements, appear very useful in particular for N_2O, for which the uncertainties of the bottom-up inventories are considerable and difficult to estimate (partly due the large spatial and temporal variability of emissions, especially from soils), which implies some risk that deficiencies of the a priori inventories may "guide" the inversion in a wrong direction.

The development and application of the N_2O inverse modelling system is performed within the framework of the European Integrated Project NitroEurope (http://www.nitroeurope.eu/) which is aiming on a detailed comparison of European CH_4 and N_2O top-down estimates from various independent inverse models.

2 Observations

The European monitoring stations used in this work are listed in Table 1, while an overview of the global station distribution is given in the Supplement in Fig. S1. The backbone of the observing system used over the global domain is ~~NOAA's~~the NOAA global cooperative air sampling network (Dlugokencky et al., 1994, Hirsch et al., 2006), providing a globally consistent dataset. In addition, we use various new regional monitoring stations over the European domain: these include quasi-continuous measurements (with a time resolution of 1 h or better) from 5 tall towers which were setup in the framework of the European RTD project CHIOTTO (http://www.chiotto.org), the AGAGE station Mace Head, the Finnish Meteorological Institute (FMI) station Pallas, the Umweltbundesamt (UBA) station Schauinsland, and the Swiss National Air Pollution Monitoring Network (NABEL)/Global Atmosphere Watch (GAW) station Jungfraujoch. Furthermore we use flask samples from Shetland Islands (operated by the Max Planck Institute – MPI, Jena).

Potential inconsistencies in the N_2O measurements, however, prevent the direct use of the combined dataset in the inversion. At 4 of the European stations, where NOAA flask samples are measured in parallel, potential offsets in the N_2O calibration can be determined directly. Comparing these NOAA flask samples with the corresponding continuous measurements coinciding within one hour, significant biases of up to 1.0 ppb are found for 3 of the 4 sites (see Table 2 and Fig. 1), of the same magnitude as the expected gradients of N_2O mixing ratios.

The N_2O measurements at the different laboratories and monitoring stations are generally performed using gas chromatography (GC) with electron capture detection (ECD). However, the setup of the instruments and calibration procedures are not standardized and differ among the different laboratories.

NOAA air samples are collected from its global cooperative air sampling network in cylindrical 2.5-L borosilicate glass flasks (see Dlugokencky et al., 1994 for details). Portable sampling systems are used to flush and fill two flasks connected in series to a pressure of 1.2 to 1.5 atmospheres. N_2O is measured by gas chromatography (GC; Hewlett-Packard 6890) with electron capture detection (ECD; anode-purged). Separation of N_2O from other components

of the sample is achieved on 5 m of HayeSep Q split into 2 columns of 2 and 3 m. The 2 m length is back-flushed to remove ECD-sensitive species that elute more slowly than N_2O. A mixture of 5% CH_4 in Ar is used as carrier gas. Samples are dried to a dew point of $\leq -70\,^{\circ}C$. The ECD response is calibrated for N_2O with a suite of standards (from 242.5 to 344.1 ppb on the NOAA-2006 scale) relative to reference air from a cylinder using an offline procedure that is separate from sample analysis. All samples are analyzed relative to the reference cylinder. N_2O mole fractions are calculated from the most recent response curve and reported in units of dry-air mole fraction, nmol/mol (abbreviated ppb). Uncertainties in the highest level standards are estimated as $\pm\,0.15\%$ of the assigned value. Repeatability of air samples – 0.4 ppb ($1\,\sigma$) – is estimated based on the average of the absolute values of the differences in N_2O mole fraction between sample pair members. This is about twice the repeatability of the analytical system – $\sim$0.2 ppb ($1\,\sigma$) estimated from repeat measurements of aliquots of natural air from a cylinder.

The methods adopted by the other laboratories differ in particular regarding the calibration procedure (see e.g. Hall et al., 2007). For instance, the CHIOTTO tall tower stations each use a set of 3–4 calibration standards based on ambient air that have been produced and of which the N_2O mixing ratios have been determined at the central laboratory of MPI-BGC (Max-Planck-Instituts für Biogeochemie) in Jena, using a N_2O scale different of that from NOAA. At Jungfraujoch each ambient air sample is bracketed with calibration runs, using real-air working standards with N_2O mixing ratios determined by cross-calibration with AGAGE standards and reported on the SIO-98 scale (Prinn et al., 2000). In general, discrepancies are mainly due to the adopted calibration method, but furthermore there are also differences in sample inlets, sample treatment, characteristics of the individual GC-ECD, or data processing. Without regular inter-comparison, no correction factors can be calculated for the scale differences, with the additional problems of the long-term drifts in the scales, so that also the relative changes between the scales need to be corrected.

An important further issue for the use of the measurements in inverse modelling is the potential influence of nearby local sources, which usually can not be realistically simulated by relatively coarse resolution atmospheric models. A very pronounced local influence is observed at the station Schauinsland (Germany), where several times per year the measured N_2O mole

fractions suddenly increase from normal values (of the order of 320 ± few ppb) to 340–380 ppb, usually associated ~~to~~with westerly winds. These N_2O spikes are very likely due to a large adipic acid production facility in Chalampe, France, at about 20 km distance to Schauinsland, for which N_2O emission of 4.96 Gg N_2O are reported for 2006. To minimize artefacts in the inversions, we rejected all data from Schauinsland above a threshold set to 330 ppb.

3 Description of the model and simulation setup

3.1 Setup of TM5 for N_2O simulations

TM5 is an offline Eulerian transport model (Krol et al., 2005) using meteorological fields from the European Centre for Medium-Range Weather Forecasts (ECMWF) Integrated Forecast System (IFS) model. It is a two-way nested zoom model, which can zoom in over the domain of interest (here Europe) at a horizontal resolution of $1° \times 1°$, embedded into the global domain, run at a resolution of $6° \times 4°$. This approach allows relatively high resolution simulations at moderate computational costs, while maintaining consistency with the global background values. In this work, the TM5 version developed for CH_4 inversions (see Bergamaschi et al., 2009, 2010, and references therein) has been modified for N_2O. We use the meteorological fields from the ERA-Interim reanalysis (Dee and Uppala, 2009, and references therein), available every 6 h over sixty vertical levels. We use a subset of 25 vertical layers (extending up to 0.2 hPa, roughly corresponding to ∼60 km height), and two zoomed domains (two-way nesting) are defined over Europe (see also Fig. S1 in the Supplement). The horizontal resolution of the global model is $6° \times 4°$, while that of the two nested domains is $3° \times 2$ and $1° \times 1°$ respectively.

For the N_2O forward simulations, three main aspects are important to consider (i) the implementation of the chemical sink in the stratosphere (ii) the a priori inventories, and (iii) the construction of the initial field of N_2O mixing ratios.

3.1.1 N_2O chemistry

N_2O is removed from the atmosphere mainly by two processes in the stratosphere, i.e. photolysis:

$$N_2O + h\,\nu \longrightarrow N_2 + O(^1D) \tag{R1}$$

and reaction with excited oxygen O(^{1}D):

$$\begin{aligned} N_2O + O(^1D) &\xrightarrow{a} NO + NO \\ N_2O + O(^1D) &\xrightarrow{b} N_2 + O_2 \end{aligned} \tag{R2}$$

Reactions (R1) and (R2) are responsible for roughly 90% and 10% of the removal respectively. These two processes can be described as function of N_2O mixing ratio as follows:

$$\frac{d}{dt}\,[N_2O]_{m,l,t} \;=\; -\,k_{m,l,t}\,[N_2O]_{m,l,t} \;-\; j_{m,l,t}\,[N_2O]_{m,l,t} \tag{R3}$$

where $[N_2O]_{m,l,t}$ represents N_2O zonal mean mixing ratio at latitude m, level l, and time t, $\frac{d}{dt}[N_2O]_{m,l,t}$ its variation in time, and $k_{m,l,t}$ and $j_{m,l,t}$ are the first-order rate coefficients for reaction with electronically excited oxygen atoms and photolysis, respectively. We use zonal mean monthly averaged values for the reaction coefficients $k_{m,l,t}$ and $j_{m,l,t}$, derived from the ECHAM5/MESSy1 model (Brühl et al., 2007). Both stratospheric reactions show a pronounced seasonality, as shown in Fig. S2 (Supplement).

In addition to the stratospheric sink, also small net surface sinks have been reported in some studies attributed to denitrification by bacteria (EPA, 2010; Hirsch et al., 2006, and references therein). The potential contribution to the global budget is not quantified, but assumed to be relatively small (Hirsch et al., 2006). Therefore this process is not considered in this study.

3.1.2 N_2O emissions

The emission inventories applied in this study as a priori estimates for the inversion consist of 13 different source categories as detailed in Table 3. Most of the anthropogenic emissions are obtained from the Emission Database for Global Atmospheric Research (EDGAR, version V4.0).

The GFEDv2 (Global Fire Emissions Database, version 2) inventory (van der Werf et al., 2004) is used to represent biomass burning emissions, and the GEIA (Global Emissions Inventory Activity) inventories are adopted for natural soil emission, enhanced soil emissions after deforestation, and ocean emissions (Bouwman et al., 1995). These emission inventories are available over the global domain at a horizontal resolution of $1^\circ \times 1^\circ$ (EDGARv4.0 data on $0.1^\circ \times 0.1^\circ$), as yearly averaged values, except biomass burning, for which monthly averaged values are reported. The total annual global emissions of our composite bottom-up inventory, equal to 13.76 Tg N_2O-N/yr, are ~15% smaller than the global total of ~16 Tg N_2O-N/yr estimated by Hirsch et al., (2006) based on simple global budget calculations (see also introduction).

3.1.3 Initial N_2O fields

The atmospheric sink is proportional to the N_2O mixing ratios (Reaction R3) and therefore directly related to the vertical profile of N_2O, which is almost constant in the troposphere and rapidly decreases with height above the tropopause. Due to the correspondence between the maximum values of the reaction coefficients of the stratospheric sinks and the maximum vertical gradient of the mixing ratio, small errors in the vertical N_2O profile can lead to large errors of its removal rates. As a consequence, a good description of the vertical N_2O profile is essential. Moreover, the lifetime of N_2O, of the order of 120 years, would require a very long model spin-up period, unless the initial field is already very close to the true state. Therefore, we used the vertical N_2O profile from the ECHAM5/MESSy1 model (Brühl et al., 2007). This profile, available as monthly averaged values (see Fig. S2, bottom panels, in the Supplement), is applied to a surface field constructed from the NOAA surface observations. These surface fields are constant in longitude and smoothed in latitude, using observations within a monthly time window, centred on the day chosen for the initial condition.

Since this field is constructed offline without using the TM5 model, however, it might not be in a sufficiently good dynamic balance within the model. Therefore, we have run the TM5-4DVAR model at coarse resolution ($6^\circ \times 4^\circ$) over the period 1999 to 2006 as spin-up period, using only surface observations from the NOAA network, and the initial N_2O field constructed as described above to initialize a first global inversion for 1999. We have then performed a series

of global inversions for the following years using as initial condition the optimized N_2O fields obtained by the previous inversion. The resulting fields from the last global inversion for 2005 are then used as initial N_2O fields for the European zoom inversions presented in this paper (running from 1 December 2005 to 1 February 2007). An important property of this initial N_2O field is its consistency with the surface observations of the NOAA network, which are used as reference for the bias correction.

3.2 Inverse modelling system

The 4DVAR inverse modelling system used in this work for N_2O is derived from the TM5-4DVAR system originally developed for CH_4 (Meirink et al., 2008; Bergamaschi et al., 2009, 2010). We refer to these papers for a detailed description of the 4DVAR system; here we describe only briefly its main characteristics (Sect. 3.2.1), and devote particular attention to the implementation of the bias correction scheme developed for the N_2O inversion (Sect. 3.2.2).

3.2.1 The TM5 4DVAR

4DVAR is a variational data assimilation technique that allows for the optimization of very large sets of parameters (described by the state vector). At the same time, very large observational datasets can be assimilated, such as satellite data or continuous surface observations. The best approximation of the true state in the space of the state vector is obtained by iteratively minimizing the cost function

$$J(\boldsymbol{x}) = \frac{1}{2}\left(\boldsymbol{x} - \boldsymbol{x}_\mathrm{b}\right)^T \mathbf{B}^{-1}\left(\boldsymbol{x} - \boldsymbol{x}_\mathrm{b}\right) + \frac{1}{2}\sum_{i=1}^{n}\left(H_i(\boldsymbol{x}) - \boldsymbol{y}_i\right)^T \mathbf{R}_i^{-1}\left(H_i(\boldsymbol{x}) - \boldsymbol{y}_i\right) \quad (1)$$

where $\boldsymbol{x}$ is the state vector, $\boldsymbol{x}_\mathrm{b}$ represents the background or first guess, i.e. the a priori estimate of the state vector, y is the set of the available observations (in the observational space), and $\mathbf{B}$ and $\mathbf{R}$ are the error covariance matrices of the ~~backgrounda~~ priori state vector and the ~~observational error covariance matrices~~observations respectively. ~~H~~$H_i(\boldsymbol{x})$ represents the observation operator ~~mapping from the state vector space to the observational space~~that provides the estimates of

the observed variables as function of $\boldsymbol{x}$. The assimilation is discretized into small assimilation time slots (index i in Eq. 1), and observed and model variables are averaged over the length of each time slot.

The length of the assimilation time slot is 3 h, while the whole inversion time window is 14 months, from 1 December 2005 to 1 February 2007. The general structure of the state vector is composed by 3 sets of variables: (1) initial state of the 3-D atmospheric N_2O mixing ratio, (2) monthly averaged emissions per model grid cell and source group and (3) bias correction parameters associated ~~to~~with different station networks, as described in detail below (Sect. 3.2.2).

To avoid negative a posteriori emissions, we apply a semi-exponential description of the probability density function (as for the CH_4 inversions; Bergamaschi et al., 2009, 2010):

$$E = E_{\mathrm{apri0}} \cdot e^x \qquad \text{for } x < 0 \tag{2}$$

$$E = E_{\mathrm{apri0}} \cdot (1 + x) \qquad \text{for } x > 0$$

where E_{apri0} are the a priori emissions (per grid cell, month and source group), and the optimization is performed as function of the parameter x, initially set to zero and described by a Gaussian distribution.

This semi-exponential probability density function introduces a weak non-linearity in the system, while all other parts of the TM5-4DVAR system are strictly linear. For the minimization of the cost function we apply the M1QN3 algorithm (Gilbert and Lemaréchal, 1989), which also effectively minimizes weakly non-linear systems.

We optimize the emissions for 4 source groups independently: soil, ocean, biomass burning, and "remaining emissions" (see Table 3). The temporal correlation coefficients for the first 3 source groups are set to zero to give the TM5-4DVAR system enough freedom to optimize the seasonality of theses sources (especially important for soil and ocean, where the bottom-up inventories provide only annual mean values). For the categories subsumed under "remaining emissions" it is assumed that the seasonal variation is rather small, and the temporal correlation is set to 9.5 months (equivalent to a month-to-month correlation coefficient of 0.9). The a priori uncertainties chosen in the control simulation are equal to 100% per grid cell, month and source

group, and the spatial correlation length is set to 200 km. As described in Sect. 3.4, different sensitivity studies for these parameters have been performed.

3.2.2 Bias correction

4DVAR is a variational method that assumes unbiased observations described by a normal distribution. Since, as described above, stations belonging to different networks may exhibit non-negligible calibration offsets, it is not possible to use the available measurements without a major modification to the scheme. This problem has been faced in the past years in numerical weather modeling, for instance at NCEP (National Centers for Environmental Prediction) by Derber and Wu (1998) and at ECMWF by Dee (2005). In the framework of inverse modeling, Bergamaschi et al. (2009) modified the same 4DVAR system used in this work to account for biases in SCIAMACHY (Scanning Imaging Absorption Spectrometer for Atmospheric CHartographY) satellite retrievals. Here we follow their method, adapted for the surface observational networks.

The 4DVAR state vector, $\boldsymbol{x}$ in Eq. (1), can be modified to include new parameters β_i describing the station biases. The modified state vector can be therefore written as $\tilde{\boldsymbol{x}} = (\boldsymbol{x}, \beta_1, \ldots, \beta_n)$, where n is the number of bias-correction parameters used. The modification of the state vector requires the observation operator H and the background error covariance matrix $\mathbf{B}$ to be changed accordingly, so that $\tilde{H}(\tilde{\boldsymbol{x}}) = \tilde{H}(\boldsymbol{x}, \boldsymbol{\beta})$ and $\mathbf{B} \rightarrow \tilde{\mathbf{B}}$. Equation (1) can therefore be written as follows:

$$J\left(\tilde{\boldsymbol{x}}\right) = \frac{1}{2}\left(\tilde{\boldsymbol{x}} - \tilde{\boldsymbol{x}}_{\mathrm{b}}\right)^{T} \tilde{\mathbf{B}}^{-1}\left(\tilde{\boldsymbol{x}} - \tilde{\boldsymbol{x}}_{\mathrm{b}}\right) + \frac{1}{2}\sum_{i=1}^{n}\left(\tilde{H}_i\left(\tilde{\boldsymbol{x}}\right) - \boldsymbol{y}_i\right)^{T} \mathbf{R}_i^{-1}\left(\tilde{H}_i\left(\tilde{\boldsymbol{x}}\right) - \boldsymbol{y}_i\right) \quad (3)$$

and the minimization performed in function of the new state vector. As stated above, stations belonging to NOAA network are considered to be the unbiased reference, assuming that no bias exists among the NOAA sites. This assumption is reasonable, since all NOAA samples are analyzed in the same laboratory using the same calibration standards.

For the other networks we have chosen independent bias parameters for each station. The major general assumption is that measurement offsets are constant in time, i.e. potential trends

in the calibration offset are not considered in this study. The a priori estimates for β_i have been set to 0 for every station, and their uncertainties to 1 ppb.

3.3 Inversion set-up

The representation of the errors associated ~~to~~with the observations is composed of two parts, i.e. the estimate of the error associated ~~to~~with the observation itself and the estimate of the uncertainty related to the capability of the model to represent the observed mixing ratios at the scales simulated by the model, the so called model representative error. We apply the same scheme as used for the CH_4 inversions (Bergamaschi et al., 2010), decomposing the total error Δy_{tot} associated ~~to~~with the observations as follows:

$$\Delta\, y_{\mathrm{tot}} \;=\; \left[\Delta\, y_{\mathrm{BL}}^2 \;+\; \Delta\, y_{\text{3-D}}^2 \;+\; \Delta\, y_t^2 \;+\; \Delta\, y_{\mathrm{OBS}}^2\right]^{1/2} \tag{4}$$

where Δy_{BL} is the estimate of the uncertainty due to the subgrid variability of emissions, applied only for stations in the boundary layer, $\Delta y_{\text{3-D}}$ is the estimate of the potential model errors ~~associated to~~due to large gradients of the mixing ratios, Δy_t is the largest standard deviation for observed or modeled mixing ratios within the 3 h time window used by the model, and Δy_{OBS} is the observational error. In this study we assume an observational error of 0.3 ppb for all observations.

As in Bergamaschi et al. (2010), in case of continuous observations only one value per day is assimilated, to avoid giving too much weight to these observations (since consecutive hourly measurements are usually correlated). After applying this "data thinning", time correlations in the observation error covariance matrix $\mathbf{R}$ are neglected, and $\mathbf{R}$ is therefore represented as a diagonal operator. In case of boundary layer stations, daytime samples are assimilated (in the window 12:00–15:00 LT) to maximize representativeness of the observations and to minimize errors related to subgrid scale effects. For mountain stations located above the boundary layer data are assimilated during night (00:00–03:00 LT) to minimize errors related to local thermal wind circulations.

3.4 Simulations

The reference inversion S1 is run as described above, using a spatial correlation coefficient for the a priori emission inventories of 200 km. In addition, various sensitivity inversions were performed to analyze the robustness of the retrieved emissions, as described in Table 4. The first two sensitivity experiments (S2 and S3 in Table 4) test the impact of different correlation lengths for the a priori emission datasets, using 300 km and 100 km values respectively. Sensitivity experiment S4 is performed to check the consistency and reliability of the bias correction system. The reference inversion includes NOAA measurements from discrete flask samples collected in parallel with the continuous measurements at 4 European sites (Table 2), resulting in very strong constraints for the bias parameters for these stations. To test the capability of the new bias scheme to satisfactorily correct measurement offsets of these stations independently from the parallel flask measurements, we run an experiment (S4) with the same configuration as S1, but without using the NOAA measurements at these four locations. Finally, in S5 we investigate the impact of the a priori emission inventory used, by replacing the standard a priori inventory by the assumption of constant, homogeneous emissions over land, and small homogeneous emissions over the ocean. Two constant emission values for land and ocean have been set with the total amounts over land and ocean equal to those of the control simulation S1. In contrast to all the other simulations only total emissions are optimized in this inversion. The uncertainty and the correlation length are set to 500% and 50 km respectively in S5 to give the system enough freedom to obtain large increments capable to relax to the information coming from the observing system.

4 Results

4.1 Global background

Although the main focus of this work is on the European scale, we discuss ~~shortly~~briefly also the results obtained for the global domain, mainly to assess the capability of the inverse modelling

system to provide realistic boundary conditions to the nested European domains. Figure S3 (Supplement) shows several global NOAA background sites, illustrating that the a posteriori simulations reproduce in general the measurements rather well. However, at the high latitude sites ALT and BRW the model simulations show some systematic bias towards higher values than observations, while at ZEP a rather good agreement is achieved. This discrepancy could point to some inconsistencies in the simulations of the stratospheric-tropospheric exchange, or in the emissions, and needs to be further clarified in subsequent studies.

The overall relatively good agreement with observations is achieved by significant inversion increments of the emissions. ~~T~~As expected, the annual global total emissions increase significantly from the apriori value of 13.76 Tg N_2O-N/yr to 16.06 Tg N_2O-N/yr (Fig. S4 in the Supplement), consistent with the estimate of $\sim$16 Tg N_2O-N/yr by Hirsch et al. (2006) for the global total emissions. We compute an atmospheric N_2O lifetime of $\sim$127 yr (total atmospheric burden/total sinks). This is in good agreement with the estimate of 122 ± 24 years derived by Volk et al. (1997), indicating that the stratospheric sink is realistically simulated in the model. The inversion increments are largely located in the tropics, consistent with the results of Hirsch et al. (2006) and Huang et al. (2008).

The natural sources represent about 62% of the global total emissions in our inversion, mainly distributed over oceans and tropical lands, broadly consistent with the estimates of Hirsch et al. (2006) (between 66% and 71%) and EPA (2010) (64%). We emphasize, however, that our estimate of natural sources largely depends on the information coming from the chosen bottom-up inventories.

4.2 European domain

4.2.1 Bias correction

Test inversions without bias correction clearly demonstrate that, despite large inversion increments, no satisfactory agreement between model simulations and observations can be achieved (results not shown). The bias correction scheme described in Sect. 3.2.2 corrects for these measurement offsets. The scheme yields very satisfactory results, reproducing the biases deter-

mined at 4 European monitoring stations from the parallel NOAA flask measurements within 0.1 ppb (Table 2). These results give us confidence that the offsets computed for the other stations are also reliable. In fact, we derive for most stations, with the exception of Mace Head and Cabauw, a non-negligible bias correction with respect to the reference NOAA network, further confirming that a bias correction scheme is a prerequisite for jointly using measurements made by independent laboratories. Very similar results were also obtained for 2007 (not shown), with the exception of the Ochsenkopf tall tower, for which a much smaller bias of 0.2 ± 0.7 ppb ($n = 11$) was derived from the parallel NOAA measurements, but which has also been well captured by the bias correction in an analogous inversion for 2007 (derived bias correction equal to 0.3 ppb).

This case illustrates that our assumption of constant biases might not be valid over longer time periods. The approach of using a constant bias correction (in contrast to a function of time), however, has the advantage of avoiding any potential interference with the signal from emissions (i.e. the risk to partially attribute an emission signal to the bias correction).

The robustness of our bias correction scheme is also confirmed by the results of the sensitivity experiments, discussed in Sect. 4.3.

4.2.2 Temporal variability of N_2O mixing ratios at monitoring stations

The inversion significantly improves the agreement of model simulations with observations, as illustrated in Fig. 2 for 5 European monitoring stations. This improvement is largely achieved by a general increase of global emissions (as discussed in Sect. 4.1), augmenting global background N_2O values, while the a priori simulations show a negative bias with respect to the observations, which increases with time. Furthermore, the inversion resolves significant seasonality of emissions (see Sect. 4.2.3), while the a priori emissions, except biomass burning, were assumed to be constant throughout the year.

Synoptic-scale variations are simulated well at most stations, e.g. Mace Head, a station which usually represents background mixing ratios, but occasionally also samples air from Ireland, UK and continental Europe. Also at more continental stations, such as Bialystok (bottom panel in Fig. 2), synoptic-scale variability is generally simulated well. However, we observe at several

of these regional continental stations slightly poorer agreement between observed and simulated high-frequency variability compared to CH_4 (Bergamaschi et al., 2010), probably due to much larger variability of N_2O emissions. In particular N_2O emissions from soils may exhibit pronounced spatial and temporal variations following changes in soil water content (rainfall), while the a priori emission inventories are constant throughout the year. Also the inversion is not capable to derive high-frequency variations of emissions, since only monthly mean values are optimized in the current system. The measurements shown in Fig. 2 are corrected with our calculated offset obtained using the bias correction scheme in the inversion (see Sects. 3.2.2. and 4.2.1), which is essential to achieve the overall good agreement with model simulations.

4.2.3 Derived emissions

Also at the European domain we see a general increase of N_2O emissions compared to a priori inventories (Fig. 3). Exceptions are UK and western Poland, where a small decrease is calculated. Total emissions over the European zoom domain increase from 1.05 TgN/yr to 1.19 TgN/yr for the control simulation. In contrast to the global emissions the percentage of emissions attributed to natural sources is much smaller, typically of the order of 10%, reaching values up to 20% in some countries of eastern Europe, and being close to zero in densely populated areas like, for instance, Benelux.

For further interpretation of results it is important to evaluate the sensitivity of the derived emissions to the available observations. For this purpose, we analyze the uncertainty reduction determined by the inverse modeling system, i.e. the ratio between a posteriori and a priori uncertainties (Fig. 4), based on an additional simulation using a conjugate gradient algorithm and the linear TM5-4DVAR system (for details see Bergamaschi et al., 2010; Meirink et al., 2008). The figure illustrates that the largest uncertainty reductions are achieved for northwest European countries and some east European countries, while hardly any uncertainty reduction is achieved for south Europe.

Therefore, we restrict in the following the discussions to countries for which the observational constraints are strongest.

In Fig. 5 and Table 5 we show the total annual emissions derived for these countries in our

inversion and compare with the emissions reported to UNFCCC (National Inventory Reports, Submission 2009, http://unfccc.int/) Since the latter cover only anthropogenic emissions we separate the estimated small contribution of natural sources from the total emissions derived in the inversion. For discussion of emissions on the European scales we use the unit Tg N_2O/yr to facilitate the comparisons with other studies on the European scale (e.g. Manning et al., 2003), while for the global studies usually the unit TgN/yr is used. In general, the derived total anthropogenic emissions agree very well with the emissions reported to UNFCCC for most countries: While for UK and Ireland our top-down estimate is about 30% lower than UNFCCC emissions, the agreement is generally better than 30% for all other countries.

This very good agreement is indeed rather surprising, since very large uncertainties are reported for the UNFCCC N_2O inventories, in general much larger than 100% (as compiled in Table ~~5~~6 for north western European countries; not shown in Fig. 5 due to the large magnitude of these uncertainties). The overall model uncertainties are estimated to be ~~of~~on the order of 40% ($2\,\sigma$), based on the calculated uncertainties (using the conjugate gradient algorithm) and taking into account potential additional model errors estimated from a preliminary model comparison performed within the NitroEurope IP project (see Table ~~6~~7). Compared to CH_4, where estimated uncertainties of bottom-up and top-down emission estimates are in the same order of magnitude, the uncertainties of the N_2O top-down estimates are obviously significantly lower than uncertainties of N_2O bottom-up inventories, demonstrating that inverse modeling can narrow down the overall uncertainties significantly. We also notice that the relatively good agreement between our derived emissions and the bottom-up inventories is consistent with the recent study of error statistics of bottom-up inventories by Leip (2010), suggesting that the present uncertainty estimates of N_2O bottom-up emission inventories are likely overestimated.

The a posteriori emissions show a remarkable seasonal variation (solid lines in Fig. 5), with a peak emission during spring ~~, very likely due~~that could be due to agricultural soil emissions affected by the use of fertilizers. The only exception to this is the Benelux area, where we observe only a secondary peak during spring, with the maximum during autumn. We emphasize, however, that the seasonal cycle of the emissions needs to be analyzed in more detail in future work, in particular considering the important role that vertical transport and Strato-

spheric-Tropospheric exchange can play in forcing it. The removal of N_2O associated to the sinks has a marked seasonal cycle and the relative importance of this processes with respect to the seasonality of surface mixing ratios needs more detailed research.

4.3 Sensitivity experiments

Spatial correlation length (S2 and S3)

In a first set of sensitivity experiments we explore the impact of the assumed spatial correlation length (Meirink et al., 2008), which was set to 200 km in the reference inversion. Increasing the correlation length to 300 km (S2) or decreasing it to 100 km (S3) has an overall only very small impact on the increments at small scales, but leads to some changes on larger scales with respect to our reference inversion S1 (Fig. S5 in the Supplement). The latter can be explained by the fact that increasing the correlation length also increases the aggregated uncertainty of the a priori emission over larger regions (since we did not modify the grid-scale uncertainty), thus allowing for a larger correction towards the observational data. The impact on the country totals, however, remains very small (Fig. 5), generally much smaller than the assumed overall uncertainty of about 40%. Furthermore, the calculated bias corrections remain very stable for these sensitivity experiments (Table 2).

Use of parallel NOAA flask samples at continuous monitoring stations (S4)

We generally include the parallel NOAA flask measurements at all continuous monitoring stations for which these flask measurements are available (4 stations). This clearly leads to very strong constraints of the calculated bias correction, since two simultaneous data sets are used for these stations. In experiment S4 we examine the robustness of the derived bias correction, when omitting the parallel flask measurements at these 4 sites. The results show derived bias corrections very close (within 0.1 ppb) to those of our reference inversion S1 (Table 2). Apparently the different stations are linked to each other via atmospheric transport, allowing rather ~~reliable~~consistent estimates of the bias correction, even if no parallel flask measurements are

available at these stations.

This gives some confidence that also the derived bias correction at other stations (where a direct experimental comparison is not available) can be considered reliable. Furthermore, S4 provides a posteriori emissions very similar to the reference inversion S1, with only minor local differences (see Fig. S6 in the Supplement).

Impact of a priori emission inventory (S5)

As expected, the inversion starting from homogeneous emissions (S5) shows larger differences compared to the reference inversion S1 (Fig. 6). The smoother pattern is explained by the fact that the a priori emission pattern is flat and the corrections can not entirely reproduce the smaller-scale patterns guided by more realistic a priori information. Setting a larger background error for emissions and a smaller correlation length compared to the reference inversion plays an important role to give the system enough degrees of freedom to retrieve regional scale emission patterns as well as possible. Overall this "free inversion" can derive emission patterns of larger regions similar to those of the other simulations within the area that is sufficiently constrained by the observational network. However the emission hotspots (attributed to industrial N_2O emissions) are not retrieved. Despite the latter shortcoming, the derived country totals are very close to the reference inversion (Fig. 5). Furthermore, the bias correction calculated in S5 is close to that obtained by the other simulations for most stations. One exception is Cabauw, for which the bias correction is significantly higher compared to all other simulations (0.6 ppb instead of 0.2 ppb). This difference is probably due to its location in the Netherlands, for which somewhat smaller emissions are derived in S5 compared to the reference inversion. This is likely due to the very high emission peak in this region that requires a very large increment when starting from the homogeneous emissions. While S5 probably slightly underestimates the Benelux emission, the system may "use" the bias correction scheme to partly compensate for this systematic error and to improve in this way the agreement with observations.

5 Conclusions

We have presented a further development of the TM5 4DVAR inverse modeling system for atmospheric N_2O. The main objective of the present study is the application of this system on the European domain, utilizing a new comprehensive data set of continuous measurements from various European monitoring stations. An important prerequisite for assimilating the data from this heterogeneous network, however, is the correction of potential measurement biases, which are directly evident from comparison with parallel NOAA measurements, available at 4 of the European stations. We demonstrated that our new bias correction scheme is capable of reproducing this experimentally derived bias within 0.1 ppb. Furthermore, we showed that virtually identical bias corrections (and emissions) are retrieved, when omitting the parallel flask measurements at these 4 sites~~, illustrating that the inter-connection of the monitoring stations via atmospheric transport strongly constrains the bias corrections.~~. This demonstrates that the monitoring stations are strongly linked via atmospheric transport, especially during synoptic situations with higher wind speeds (when emissions have a smaller impact on the mixing ratios, and the mixing ratios are close to the baselines of the stations). During the inversion period (14 months) many different synoptic situations are encountered (e.g. situations where air masses are transported from station A to B, but also from B to A). This apparently allows the inversion system to differentiate between differences of mixing ratios (station B - station A) arising from emissions between the stations (which depend on the wind direction) and differences arising from the calibration offset (which are independent of the wind direction / synoptic situation). The use of bias correction implies that the inversion system cannot derive any information from the spatial gradient between the stations (for those stations which have independent bias corrections), but utilize the information within the footprint of each station independently, while the bias correction allows to make the measurements consistent with each other. However, the global NOAA flask sampling network is essential for the realistic simulations of the global emissions, and as reference which can be assumed to be un-biased. We emphasize that the very encouraging bias corrections do not replace systematic comparisons of standards and measurements, which are crucial to improve the consistency of the measurements from different sites and independent laboratories. In this study we made the simple assumption that the measurement bias is constant

in time and can be described by a constant offset. While this approach seems to be able to correct for a significant part of the measurement biases, the systematic errors may have in reality a more complex structure. Eg., the measurement bias may have additional components varying in time, which are difficult to be quantified by the inverse modelling system in the absence of additional information about the underlying processes leading to the biases. In addition, the biases may also depend on the N_2O mixing ratios (given the non-linear response function of the currently used ECD detectors). Hence, further improvement of the measurements is indispensable to improve the top-down emission estimates in the future.

Total anthropogenic emissions derived by the TM5-4DVAR system for the northwest European and several east European countries agree well with bottom-up inventories reported to UNFCCC, with much smaller differences than the very large uncertainties of the UNFCCC estimates. Furthermore, the estimated model uncertainties (of the order of 40%) are much smaller than the uncertainties of the UNFCCC estimates, currently estimated to be larger than 100% for most European countries. This illustrates that atmospheric observations combined with inverse modeling can significantly decrease the uncertainties of N_2O emissions.

Finally, we demonstrated that our "free inversion" (sensitivity experiment S5 starting from homogenous emissions), yields larger scale regional emission patterns very similar to the reference inversion (guided by detailed a priori emission inventories) within the area constrained by the network. An exception, however, is the pronounced emission peaks related to industrial N_2O emissions (adipic acid production), which are typically smeared out over much larger regions in inversion S5. The country totals derived in S5, however, are generally very close to the reference inversion, illustrating the potential of completely independent top down verification of bottom up emission inventories, avoiding the use of detailed a priori information. This is considered very important especially for N_2O, for which bottom-up inventories have still considerable uncertainties, hence bearing the risk that using these inventories may guide the inversion in a wrong direction in some cases.

Further improved top-down emission estimates are expected from the ongoing detailed model intercomparison performed within the NitroEurope project, involving 5 independent inverse models. In addition, this intercomparison will provide more realistic estimates of overall uncer-

tainties of top-down emission estimates.

Supplementary material related to this article is available online at: http://\@journalurl/\@pvol/\@fpage/\@pyear/\@journalnameshortlower-\@pvol-\@fpage-\@pyear-supplement.pdf.

Acknowledgements. We thank Suvi Monni and John van Aardenne for discussions and support with the EDGARv4.0 database. We are grateful to Adrian Leip and Bernd Gugele for discussion of uncertainties of UNFCCC emissions. We thank Arjo Segers for support of the TM5 modeling framework and for preprocessing the ECMWF meteo data. This work has been supported by the European Commission RTD project NitroEurope-IP, contract number 017841-2, 6th Framework Programme. We are grateful to Ronnie Robertson for his diligent flask sampling at Sumburgh Head, Shetland Isles, and to Martin Heimann for processing and screening the sampled data at this site. The Swiss National Air Pollution Monitoring Network (NABEL) is run by Empa in joint collaboration with the Swiss Federal Office for the Environment. We thank Zoltán Barcza, and István Szilágyi for their sampling at Hegyhátsál. Significant support for the operation of Hegyhátsál has been provided by the Hungarian Scientific Research Fund (project number CK77550).

[UNFCCC reference has been added]

References

Bergamaschi, P.: Atmospheric Monitoring and Inverse Modelling for Verification of National and EU Bottom-up GHG Inventories – report of the workshop "Atmospheric Monitoring and Inverse Modelling for Verification of National and EU Bottom-up GHG Inventories" under the mandate of Climate Change Committee Working Group I, Casa Don Guanella, European Commission Joint Research Centre, Institute for Environment and Sustainability, 8–9 March 2007, Ispra, Italy, 153 pp., 2007.

Bergamaschi, P., Frankenberg, C., Meirink, J. F., Krol, M., Villani, M. G., Houweling, S., Dentener, F., Dlugokencky, E. J., Miller, J. B., Gatti, L. V., Engel, A., and Levin, I.: Inverse modeling of global and regional CH_4 emissions using SCIAMACHY satellite retrievals, J. Geophys. Res., 114, D22301, doi:10.1029/2009JD012287, 2009.

Bergamaschi, P., Krol, M., Meirink, J. F., Dentener, F., Segers, A., van Aardenne, J., Monni, S., Vermeulen, A., Schmidt, M., Ramonet, M., Yver, C., Meinhardt, F., Nisbet, E. G., Fisher, R., O'Doherty,

S., and Dlugokencky, E. J.: Inverse modeling of European CH_4 emissions 2001–2006, J. Geophys. Res., 115, D22309, doi:10.1029/2010JD014180, 2010.

Bouwman, A. F., Van der Hoek, K. W., and Olivier, J. G. J.: Uncertainties in the global source distribution of nitrous oxide, J. Geophys. Res., 100, 2785–2800, 1995.

Brühl, C., Steil, B., Stiller, G., Funke, B., and Jöckel, P.: Nitrogen compounds and ozone in the stratosphere: comparison of MIPAS satellite data with the chemistry climate model ECHAM5/MESSy1, Atmos. Chem. Phys., 7, 5585–5598, doi:10.5194/acp-7-5585-2007, 2007.

Crutzen, P. J.: Estimates of possible variations in total ozone due to natural causes and human activities, Ambio, 3, 201–210, 1974.

Dee, D. P.: Bias and Data Assimilation, Q. J. Roy. Meteor. Soc., 131, 3323–3343, 2005.

Dee, D. P. and Uppala, S.: Variational bias correction of satellite radiance data in the ERA-Interim reanalysis, Q. J. Roy. Meteor. Soc., 135, 1830–1841, 2009.

Derber, J. C. and Wu, W.-S.: The use of TOVS clud-cleared radiances in the NCEP SSI analysis system, Mon. Weather Rev., 126, 2287–2299, 1998.

Dlugokencky, E. J., Steele, L. P., Lang, P. M., and Masarie, K. A.: The growth rate and distribution of atmospheric methane, J. Geophys. Res., 99, 17021–17043, 1994.

EPA: Methane and Nitrous Oxide Emissions From Natural Sources, Office of Atmospheric Programs, EPA 430-R-10-001, 194 pp., available as pdf: http://www.epa.gov/methane/pdfs/Methane-and-Nitrous-Oxide-Emissions-From-Natural-Sources.pdf, last access: November 2010.

Gilbert, J. C. and Lemaréchal, C.: Some numerical experiments with variable-storage quasi-Newton algorithms, Math. Program., 45, 407–435, 1989.

Hall, B., Dutton, G., and Elkins, J.: The NOAA nitrous oxide standard scale for atmospheric observations, J. Geophys. Res., 112, D09305, doi:10.1029/2006JD007954, 2007.

Hall, B. D., Butler, J. H. D. C. A., Dutton, G. S., Elkins, J. W., Hurst, D. F., King, D. B., Kline, E. S., Lind, J., Lock, L. T., Mondeel, D., Montzka, S. A., Moore, F. L., Nance, J. D., Ray, E. A., Romashkin, P. A., and Thompson, T. M.: Halocarbons and other atmospheric trace species, in: Climate Monitoring and Diagnostics Laboratory CMDL No. 26 Summary Report 2000–2001, edited by: King, D. B., Schnell, R. C., Rosson, R. M., and Sweet, C., NOAA Oceanic and Atmos. Res., Boulder, CO, 106–135, 2002.

Hirsch, A. I., Michalak, A. M., Bruhwiler, L. M., Peters, W., Dlugokencky, E. J., and Tans, P. P.: Inverse modeling estimates of the global nitrous oxide surface flux from 1998–2001, Global Biogeochem. Cy., 20, GB1008, doi:10.1029/2004GB002443, 2006.

Huang, J., Golombek, A., Prinn, R., Weiss, R., Fraser, P., Simmonds, P., Dlugokencky, E., Hall, B., Elkins, J., Steele, P., Langenfelds, R., Krummel, P., Dutton, G., and Porter, L.: Estimation of regional

emissions of nitrous oxide from 1997 to 2005 using multinetwork measurements, a chemical transport model, and an inverse method, J. Geophys. Res., 113, D17313, doi:10.1029/2007JD009381, 2008.

IPCC: Good Practice Guidance and Uncertainty Management in National Greenhouse Gas Inventories, edited by: Penman, J., Kruger, D., Galbally, I., Hiraishi, T., Nyenzi, B., Emmanul, S., Buendia, L., Hoppaus, R., Martinsen, T., Meijer, J., Miwa, K., and Tanabe, K., published for the IPCC by the Institute for Global Environmental Strategies, Japan, 2000.

IPCC: Climate Change 2007: The Physical Science Basis, Contribution of Working Group I to the Fourth Assessment Report of the Intergovernmental Panel on Climate Change, Cambridge University Press, Cambridge, UK and New York, NY, USA, 996 pp., 2007.

Krol, M., Houweling, S., Bregman, B., van den Broek, M., Segers, A., van Velthoven, P., Peters, W., Dentener, F., and Bergamaschi, P.: The two-way nested global chemistry-transport zoom model TM5: algorithm and applications, Atmos. Chem. Phys., 5, 417–432, doi:10.5194/acp-5-417-2005, 2005.

Leip, A.: Quantitative quality assessment of the greenhouse gas inventory for agriculture in Europe, Climatic Change, 103(1–2), 245–261, doi:10.1007/s10584-010-9915-5, 2010.

Manning, A. J., Ryall, D. B., Derwent, R. G., Simmonds, P. G., and O'Doherty, S.: Estimating European emissions of ozone-depleting and greenhouse gases using observations and a modeling back-attribution technique, J. Geophys. Res., 108, 4405, doi:4410.1029/2002JD002312, 2003.

Meirink, J. F., Bergamaschi, P., and Krol, M. C.: Four-dimensional variational data assimilation for inverse modelling of atmospheric methane emissions: method and comparison with synthesis inversion, Atmos. Chem. Phys., 8, 6341–6353, doi:10.5194/acp-8-6341-2008, 2008.

Messager, C., Schmidt, M., Ramonet, M., Bousquet, P., Simmonds, P., Manning, A., Kazan, V., Spain, G., Jennings, S. G., and Ciais, P.: Ten years of CO_2, CH_4, CO and N_2O fluxes over Western Europe inferred from atmospheric measurements at Mace Head, Ireland, Atmos. Chem. Phys. Discuss., 8, 1191–1237, doi:10.5194/acpd-8-1191-2008, 2008.

Nevison, C. D. and Holland, E.: A re-examination of the impact of anthropogenically fixed nitrogen on atmospheric N_2O and the statospheric O_3 layer, J. Geophys. Res., 103, 25519–25536, 1997.

Prinn, R., Cunnold, D., Rasmussen, R., Simmonds, P., Alyea, F., Crawford, A., Fraser, P., and Rosen, R.: Atmospheric Emissions and Trends of Nitrous Oxide Deduced From 10 Years of ALE-GAGE Data, J. Geophys. Res., 95, 18369–18385, 1990.

Prinn, R. G., Weiss, R. F., Fraser, P. J., Simmonds, P. G., Cunnold, D. M., Alyea, F. N., O'Doherty, S., Salameh, P., Miller, B. R., Huang, J., Wang, R. H. J., Hartley, D. E., Harth, C., Steele, L. P., Sturrock, G., Midgley, P. M., and McCulloch, A.: A history of chemically and radiatively important gases in air deduced from ALE/GAGE/AGAGE, J. Geophys. Res., 105, 17751–17792, 2000.

Ravishankara, A. R., Daniel, J. S., and Portmann, R. W.: Nitrous Oxide (N_2O): The Dominant Ozone-Depleting Substance Emitted in the 21st Century, Science, 326, 123–125, 2009.

Ryall, D. B., Derwent, R. G., Manning, A. J., Simmonds, P. G., and O'Doherty, S.: Estimating source regions of European emissions of trace gases from observations at Mace Head, Atmos. Environ., 35, 2507–2523, 2001.

UNFCCC, Updated UNFCCC reporting guidelines on annual inventories following incorporation of the provisions of decision 14/CP.11. Note by the secretariat, United Nations Office at Geneva, Geneva, FCCC/SBSTA/2006/9, 93pp, 2006.

van der Werf, G. R., Randerson, J. T., Collatz, G. J., Giglio, L., Kasibhatla, P. S., Arellano Jr., A. F., Olsen, S. C., and Kasischke, E. S.: Continental-Scale Partitioning of Fire Emissions During the 1997 to 2001 El Nino/LaNina Period, Science, 303, 73–76, 2004.

Volk, C. M., Elkins, J. W., Fahey, D. W., Dutton, G. S., Gilligan, J. M., Loewenstein, M., Podolske, J. R., Chan, K. R., and Gunson, M. R.: Evaluation of source gas lifetimes from stratospheric observations, J. Geophys. Res., 102, 25543–25564, 1997.

Table 1. List of stations used in the inversions. Only stations in the European zoomed domains are listed here (for the global stations see Fig. S1 in the Supplement). Latitude, longitude, altitude and type of sampling (Flask or Continuous) are listed. Stations with grey background are used in the inversion in all simulations but S4. Positive/negative latitudes and longitudes indicate north/south and east/west, respectively.

Id_obs	Network	Lat	Lon	Alt	Tp	Station Name
PAL	NOAA	67.97	24.12	560	F	Pallas, Finland
PAL	FMI	67.97	24.12	560	C	Pallas, Finland
STM	NOAA	66.00	2.00	5	F	Ocean station M, Norway
ICE	NOAA	63.34	−20.29	127	F	Heimay, Vestmannaeyjar, Iceland
TT1	CHIOTTO	56.55	−2.98	535	C	Angus, UK, base: 313 m, tower level: 222 m
BAL	NOAA	55.35	17.22	28	F	Baltic Sea, Poland
SIS	MPI	59.85	1.27	46	F	Shetland Island, UK
MHD	AGAGE	53.33	−9.90	25	C	Mace Head, Ireland
MHD	NOAA	53.33	−9.90	25	F	Mace Head, Ireland
BI5	CHIOTTO	52.25	22.75	460	C	Bialystok, Poland, base: 160 m, tower level:300 m
CB4	CHIOTTO	51.97	4.93	198	C	Cabauw, Netherlands, base: −2 m, tower l.: 200 m
OX3	CHIOTTO	50.05	11.82	1185	C	Ochsenkopf, Germany, base: 1022 m, tower l.: 163 m
OXK	NOAA	50.05	11.82	1185	F	Ochsenkopf, Germany, base: 1022 m, tower l.: 163 m
SIL	UBA	47.91	7.91	1205	C	Schauinsland, Germany
HPB	NOAA	47.80	11.01	985	F	Hohenpeissenberg, Germany
HU1	CHIOTTO	46.95	16.65	344	C	Hegyhatsal, Hungary, base: 248 m, tower level: 96 m
HUN	NOAA	46.95	16.65	344	F	Hegyhatsal, Hungary, base: 248 m, tower level: 96 m
JFI	NABEL	46.55	7.98	3580	C	Jungfraujoch, Switzerland
BSC	NOAA	44.17	28.68	3	F	Black Sea, Constanta, Romania
AZR	NOAA	38.77	−27.38	40	F	Terceira Island, Azores, Portugal
LMP	NOAA	35.52	12.63	45	F	Lampedusa, Italy
WIS	NOAA	31.13	34.88	400	F	Sede Boker, Negev Desert, Israel
IZO	NOAA	28.30	−16.48	2360	F	Tenerife, Canary Islands, Spain
ASK	NOAA	23.18	5.42	2728	F	Assekrem, Algeria

Table 2. Bias corrections for the different European stations. The second column indicates the corresponding network or laboratory. Note however, that all CHIOTTO tall towers (CHI) are treated independently regarding the bias correction. The third column gives the average bias and standard deviation in units of ppb derived from the comparison with the NOAA flask samples which are available at 4 stations (station data minus NOAA data). n represents the number data pairs (measurements coinciding within 1 h). The subsequent columns give the bias corrections derived from the different inversions (units are parts per billion - ppb - dry-air mole fraction).

Station	network/ laboratory	Comparison with NOAA	S1	S2	S3	S4	S5
Pallas	FMI	0.5 ± 0.3 ($n = 36$)	0.5	0.5	0.5	0.5	0.5
Shetland Island	MPI		0.5	0.5	0.5	0.5	0.6
Angus	CHIOTTO		0.8	0.8	0.8	0.8	0.8
Mace Head	AGAGE	~~-0.1~~0.1 ± 0.3 ($n = 36$)	0.0	0.0	0.0	-0.1	0.0
Bialystok	CHIOTTO		0.3	0.2	0.3	0.3	0.4
Cabauw	CHIOTTO		0.2	0.2	0.2	0.2	0.6
Ochsenkopf	CHIOTTO	$1.0 \pm$ ~~0.4~~0.3 ($n = 5$)	1.1	1.1	1.1	1.1	1.2
Schauinsland	UBA		0.4	0.4	0.5	0.4	0.5
Hegyhatsal	CHIOTTO	1.0 ± 1.2 ($n = 23$)	1.0	1.0	1.1	1.1	1.1
Jungfraujoch	NABEL		-0.4	-0.4	-0.4	-0.4	-0.4

Table 3. Emission inventories used as a priori estimate in the inversion. Units for total emissions are Tg N/yr for column 3 and Tg N_2O/yr for column 4. Emission categories are assigned to 4 source groups compiled in the last column, which are optimized independently in the inversions.

Category	Source	Total (N_2O-N) Emissions	Total (N_2O) Emissions	Monthly Variations	Inversion category
Natural Soil	GEIA	4.59	7.21	N	Soil
Agricultural Soil	EDGAR 4.0	3.24	5.09	N	Soil
Manure	EDGAR 4.0	0.21	0.33	N	Remaining emissions
Biomass Burning	GFED v2	0.65	1.02	Y	Biomass burning
Enhanced soil emis. after deforestation	GEIA	0.36	0.57	N	Remaining emissions
Agricultural Burning	EDGAR 4.0	0.02	0.03	N	Remaining emissions
Transport	EDGAR 4.0	0.16	0.25	N	Remaining emissions
Residential	EDGAR 4.0	0.11	0.17	N	Remaining emissions
Industrial	EDGAR 4.0	0.38	0.60	N	Remaining emissions
Energy-Manufacture	EDGAR 4.0	0.21	0.33	N	Remaining emissions
Oil-Gas Production	EDGAR 4.0	< 0.01	< 0.01	N	Remaining emissions
Waste	EDGAR 4.0	0.22	0.35	N	Remaining emissions
Ocean	GEIA	3.60	5.66	N	Ocean
Total	–	13.76	21.62	Y	

Table 4. List of the experiments described in this work. L_corr denotes the spatial correlation length applied for the emissions.

Inversion	L_corr	Description
S1	200 km	Reference inversion
S2	300 km	As S1, but spatial correlation length 300 km
S3	100 km	As S1, but spatial correlation length 100 km
S4	200 km	As S1, without using the parallel NOAA measurements at 4 European stations
S5	50 km	As S1, but homogeneous a priori emissions (two different values over land and over ocean, respectively). Spatial correlation length 50 km, and uncertainty of emissions set to 500%. Only total emissions optimized.

Table 5. 2006 total N_2O emissions (Tg N_2O/yr) for the same countries and regions shown in Fig. 5. Natural and anthropogenic emissions are separated in order to allow for a clear comparison with UNFCCC data.

	UNFCCC	A priori Anthropogenic	A priori Natural	S1 Total	S1 Anthropogenic	S5 Total
Germany	0.17	0.17	0.01	0.21	0.20	0.18
France	0.21	0.14	0.01	0.20	0.18	0.18
Benelux	0.09	0.06	0.00	0.08	0.08	0.06
UK, Ireland	0.14	0.11	0.01	0.10	0.09	0.08
North-western Europe	0.60	0.48	0.03	0.59	0.55	0.51
Poland	0.10	0.09	0.01	0.11	0.10	0.08
Czech R., Slovakia, Hungary	0.07	0.06	0.00	0.09	0.08	0.08
Eastern Europe	0.17	0.15	0.01	0.19	0.18	0.16
North-central Europe	0.77	0.63	0.04	0.78	0.73	0.66

Table 6. Uncertainty estimates ($2\,\sigma$) for emissions reported to UNFCCC for the north-western Europe countries (NWE: Germany, France, Benelux, UK and Ireland).

		UK	IRE	NL	BEL	France	Germany	NWE[4]
Fuel combustion								
emission (2006)	Tg N_2O/yr	0.012	0.003	0.001	0.001	0.010	0.017	0.044
rel. uncertainty	%	195.0	50.0	50.1	442.8	20.2	36.7	86.4
abs. uncertainty	Tg N_2O/yr	0.023	0.002	0.001	0.004	0.002	0.006	0.038
Road transport								
emission (2006)	Tg N_2O/yr	0.005	0.001	0.001	0.003	0.002	0.004	0.016
rel. uncertainty	%	170.0	25.0	50.2	100.1	3.2	38.8	93.8
abs. uncertainty	Tg N_2O/yr	0.009	0.000	0.001	0.003	0.000	0.002	0.015
Industrial processes								
emission (2006)	Tg N_2O/yr	0.008	0.000	0.020	0.008	0.019	0.037	0.092
rel. uncertainty	%	20.1	10.0	23.0	65.8	25.2	39.3	34.8
abs. uncertainty	Tg N_2O/yr	0.002	0.000	0.005	0.005	0.005	0.015	0.032
agricultural soils								
emission (2006)	Tg N_2O/yr	0.078	0.021	0.028	0.013	0.153	0.091	0.384
rel. uncertainty	%	424.0	57.9	82.8	251.8	200.2	306.6	256.3
abs. uncertainty	Tg N_2O/yr	0.331	0.012	0.023	0.033	0.306	0.279	0.984
manure management								
emission (2006)	Tg N_2O/yr	0.006	0.001	0.003	0.003	0.019	0.008	0.040
rel. uncertainty	%	414.0	100.6	100.5	90.6	50.2	20.9	107.5
abs. uncertainty	Tg N_2O/yr	0.024	0.001	0.003	0.003	0.010	0.002	0.043
waste water								
emission (2006)	Tg N_2O/yr	0.004	0.000	0.001	0.001	0.003	0.009	0.018
rel. uncertainty	%	401.1	14.1	53.9	111.8	104.4	75.0	155.5
abs. uncertainty	Tg N_2O/yr	0.016	0.000	0.001	0.001	0.003	0.007	0.028
total								
total major categories[1]	Tg N_2O/yr	0.113	0.026	0.054	0.029	0.206	0.166	0.594
total all anthropogenic[2]	Tg N_2O/yr	0.113	0.027	0.055	0.029	0.210	0.169	0.603
total uncertainty[3]	Tg N_2O/yr	0.333	0.012	0.024	0.034	0.306	0.280	0.987
relative uncertainty[3]	%	294.7	46.2	44.4	117.2	148.5	168.7	166.2

[1] "Major categories" are the individual categories listed in the table.

[2] Country total of all anthropogenic emissions as reported to UNFCCC (2006).

[3] Uncertainty of total emissions estimated from the uncertainties given for the listed major individual source categories, assuming no correlation among the errors of different categories.

[4] for aggregation of uncertainties for emissions from individual countries to the NWE uncertainties, correlated errors are assumed (for emissions of same categories). In reality, the errors may be only partially correlated.

Table 7. Uncertainty estimates for emissions derived by the TM5-4DVAR inverse modeling system. The Potential additional model errors are estimated from a preliminary model comparison performed within the NitroEurope IP project.

	Calculated uncertainty %	Potential additional error %	Overall uncertainty %
Germany	16.0	~ 30	~ 34
France	18.1	~ 30	~ 35
Benelux	29.2	~ 30	~ 42
UK Ireland	31.4	~ 30	~ 43
North western Europe	8.9	~ 30	~ 31
Poland	26.2	~ 30	~ 40
Czech R., Slovakia, Hungary	22.2	~ 30	~ 37
Eastern Europe	20.5	~ 30	~ 35
North central Europe	7.4	~ 30	~ 31

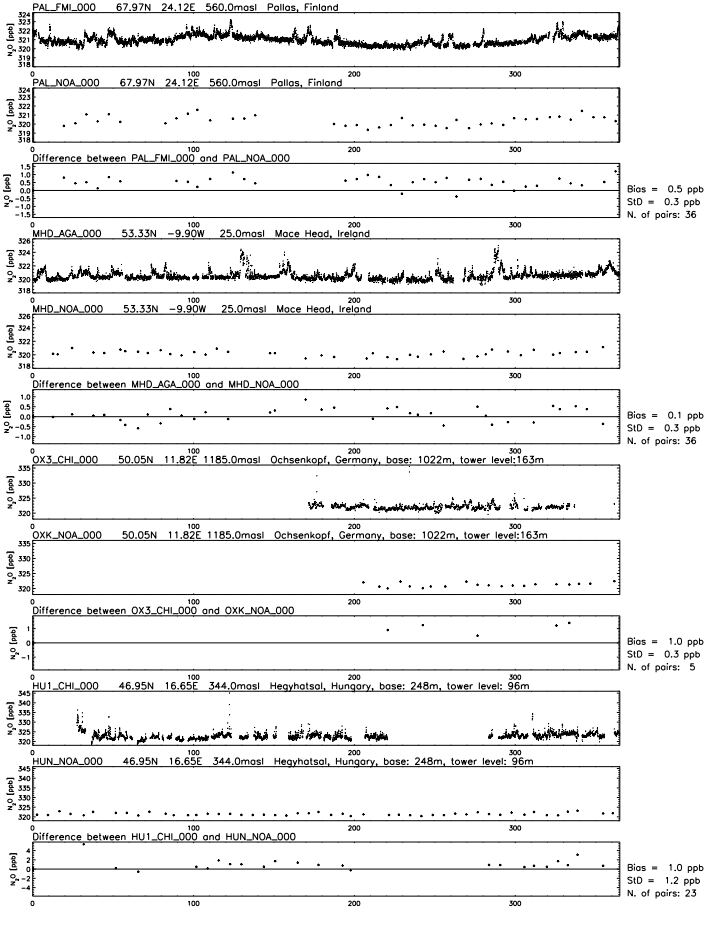

Fig. 1. N_2O mixing ratio at the 4 locations where parallel measurements are available. For each location, the first panel represents continuous measurements, the second panel NOAA flask samples. Their difference of measurements coinciding within 1 h is shown in the third panel. The calculated bias, standard deviation, and number of pairs are reported for each station.

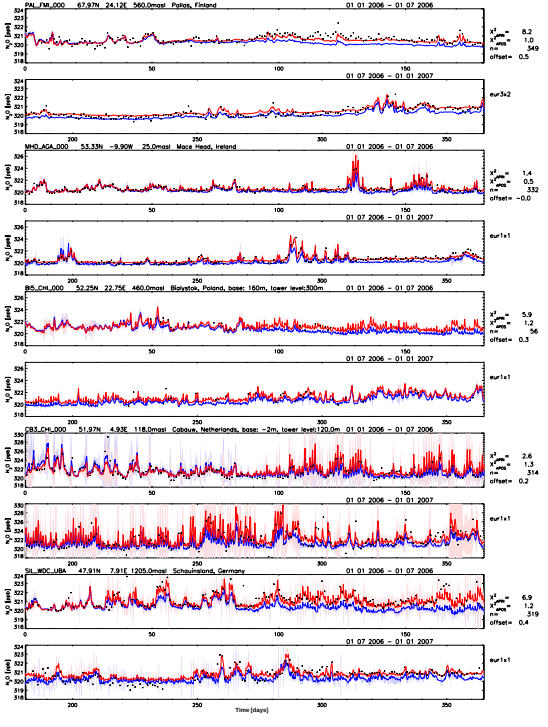

Fig. 2. Time series (days) of observed and simulated N_2O mixing ratios at 5 of the available European stations: Pallas, Mace Head, Bialystok, Cabauw, and Schauinsland. One year of data, from 1 January to 31 December 2006, is split into two 6-month panels for each station. Blue lines represent a priori simulations and red lines are a posteriori simulations for the reference inversion S1. Shaded areas represent estimated uncertainties of the model simulations. Measurements are shown as black dots. The calculated bias corrections (offset) are given on the right of each panel and have been subtracted from the measurements. Units are ppb.

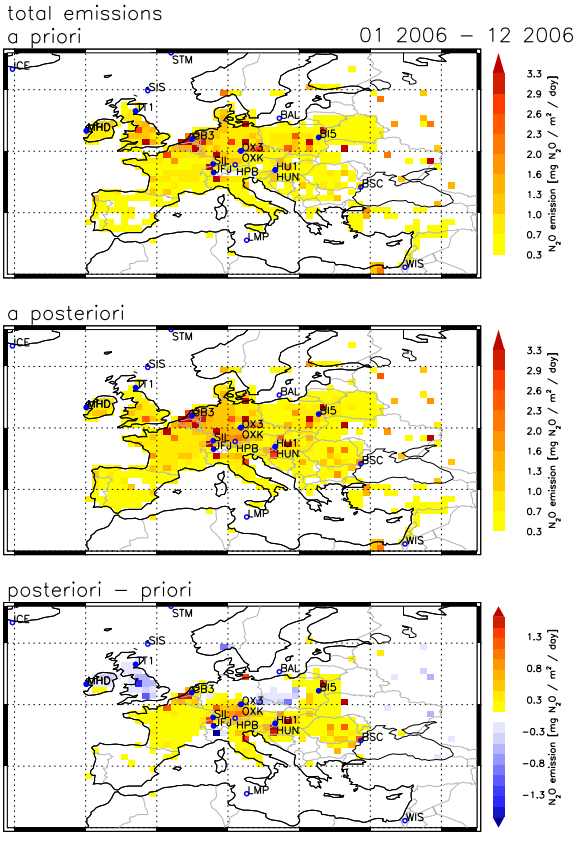

Fig. 3. A priori (top panel) and a posteriori (mid panel) emissions over the European domain (annual mean emissions for 2006). Bottom panel represents the difference between the two fields (a posteriori - a priori). Filled circles represent stations which take continuous measurements, open circles sites those with flask measurements.

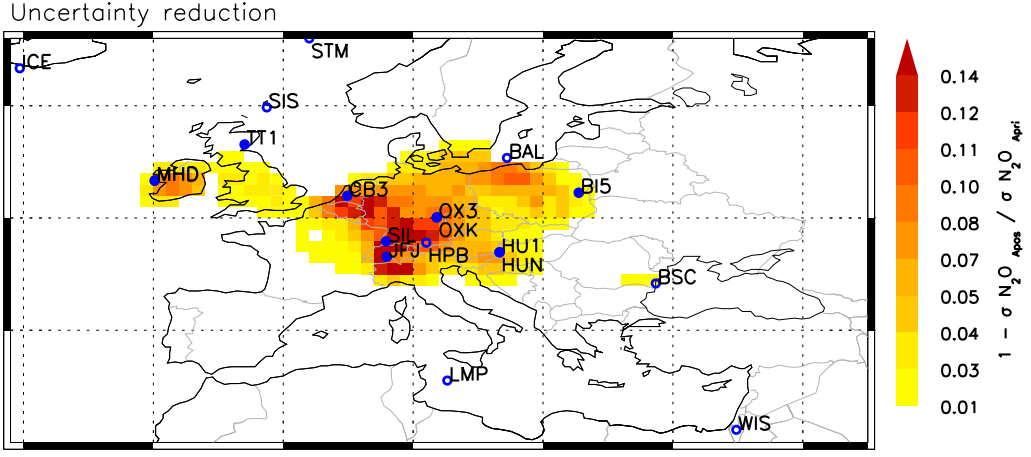

Fig. 4. Calculated ~~R~~reduction of uncertainties of emissions per grid cell ($1-\sigma_{\mathrm{N_2O_{apos}}}/\sigma_{\mathrm{N_2O_{apri}}}$). Allowed values are in the interval $[0,1]$, 0 indicating that the a posteriori uncertainty is equal to the a priori uncertainty (no reduction), 1 indicating a perfect uncertainty reduction.

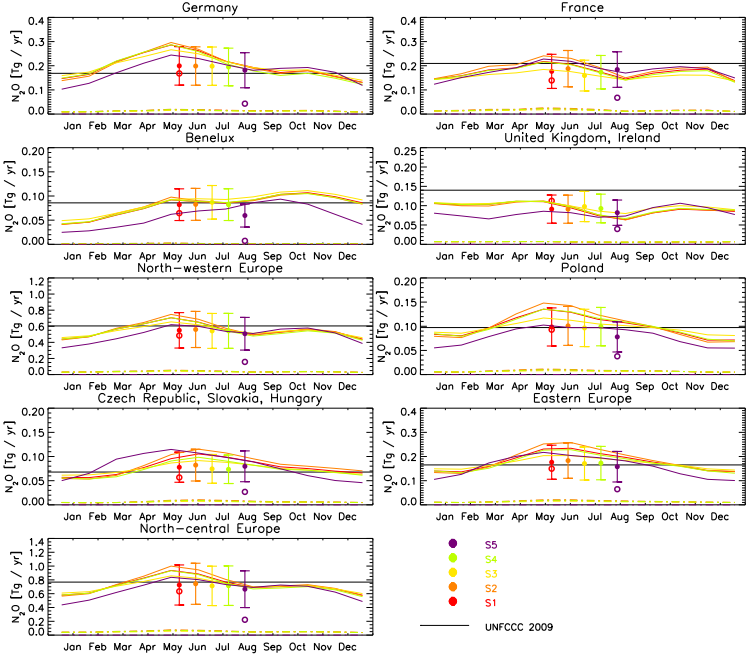

Fig. 5. Total emissions for various northwest European and east European countries for 2006 (see also Table 5). The filled colored circles represent the ~~results~~annual total emissions from the 5 inversions and open circles are the applied a priori emissions. The small natural emissions have been subtracted for S1–S4 (while this is not possible for S5, which does not use any detailed a priori knowledge). Emissions reported to UNFCCC are shown by the black solid line (uncertainties of the order of 150% are not shown here, but compiled in Table ~~5~~6). North-western Europe represents the sum for Germany, France, Benelux, United Kingdom and Ireland, while Eastern Europe represents the sum of Poland, Czech Republic, Slovakia, and Hungary. Finally North-central Europe represents the sum of all considered countries. Colored solid lines represent the seasonal variation of anthropogenic emissions derived in the inversions (3 month running mean), while the colored dash-dotted lines show the small contribution from natural sources.

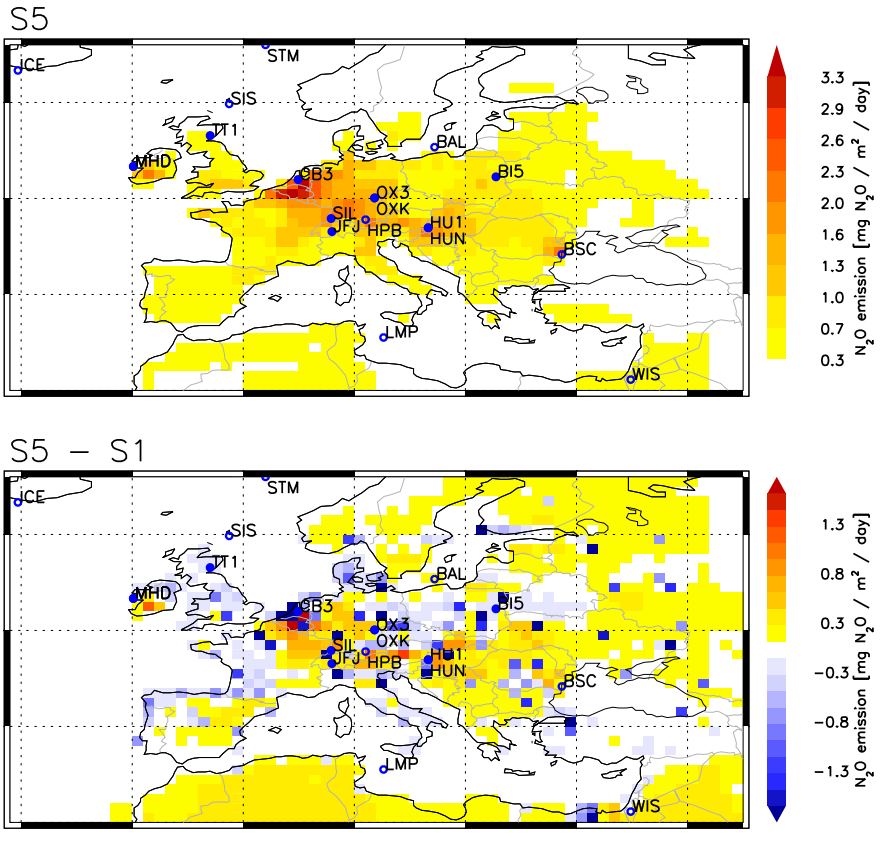

Fig. 6. A posteriori emissions for S5 (top panel) and difference to reference inversion S1 (mid panel of Fig. 3).